Chemical Engineering Journal 161 (2010) 9–18

Contents lists available at ScienceDirect

Chemical Engineering Journal

journal homepage: www.elsevier.com/locate/cej

Modeling virus transport and inactivation in a fluoropolymer tube UV photoreactor using Computational Fluid Dynamics

Ferdinando Crapulli[a], Domenico Santoro[b,*], Charles N. Haas[c], Michele Notarnicola[a], Lorenzo Liberti[a]

[a] Politecnico di Bari, Via De Gasperi, Taranto 74100, Italy
[b] University of Western Ontario, Richmond Street, London Ontario, Canada N6A 5B9
[c] Drexel University, Chestnut Street, Philadelphia 19104, PA, USA

ARTICLE INFO

Article history:
Received 2 February 2010
Received in revised form 31 March 2010
Accepted 31 March 2010

Keywords:
Bacteriophages
Computational Fluid Dynamics
Disinfection
Fluoropolymer
Photoreactor
Ultraviolet

ABSTRACT

Fluoropolymer tube photoreactors employing external UV lamps to irradiate the fluid conveyed by semi-transparent tubes are currently used for water and wastewater applications based on their intrinsic simplicity in system assembly and claims that the hydrophobic characteristics of the tube material reduce fouling. Nonetheless, there is limited published information to date on the short and long term disinfection efficiency and the potential implications of these factors for operational costs.In this paper, empirical and numerical bioassay experiments on virus inactivation were conducted on a pilot-scale fluoropolymer tube photoreactor using MS2 and T1 bacteriophages to gain further insight into delivered dose. Simulated and observed MS2 and T1 reduction equivalent doses displayed good agreement with an error (relative to the observed RED) ranging from −13.7% to +4.4% for MS2 (average = −3.9%) and from −5.6% to +27.0% for T1 (average = +4.6%).The impact of the fluoropolymer UV absorption on disinfection was also assessed. Integrating sphere measurements revealed that absorption events occurring in the fluoropolymer tubes play a pivotal role in determining disinfection efficiency. At 253.7 nm, the diffuse transmission of UV light was the dominant radiative transfer mechanism and a considerable proportion of incident photon flux (13.5%) was absorbed by the fluoropolymer tube. As highlighted by the model sensitivity analysis, the fluoropolymer absorption coefficient was found to be the most important factor affecting bacteriophage inactivation.Although further research will be conducted to investigate potential efficiency enhancements attainable through shape optimization and internal UV reflectors, CFD predictions indicated that the current electrical efficiency of the investigated photoreactor (0.0190–0.0289 kWh m^{-3} MS2 log^{-1}) was considerably higher than conventional UV photoreactors (0.0044–0.0049 kWh m^{-3} MS2 log^{-1}) suggesting that fluoropolymer tube UV technologies may not be ideal for high-flow installations or energy sensitive applications.

1. Introduction

The occurrence of disinfection by-products formed by chemical oxidation of organics in water and wastewater [1,2] has suggested that alternative, environmentally friendly disinfection techniques should be considered and investigated [3,4]. Among physical disinfection processes, UV disinfection – introduced in 1877 [5] and popular since the 1980s [6] – has emerged as a cost-effective means to inactivate a wide range of microorganisms [7–9]. Due to the demonstrated sensitivity of the UV disinfection performance to reactor hydraulics [10], several alternative reactor configurations have been proposed to date. The configurations can be classified, for example, according to the relative lamp-to-liquid location (e.g., immersed in the fluid or external to the fluid) and orientation (parallel to flow or cross flow).

While liquid-immersed UV lamp reactors using quartz sleeves surrounding the lamp have received considerable attention [10–16], fewer studies are available on fluoropolymer tube photoreactors [17,18] albeit their potential advantages over conventional technologies such as an intrinsic simplicity in system assembly, easy of operation, a lower risk of lamp breakage and claims that the hydrophobic characteristics of the tube material may reduce fouling [19]. Moreover, these studies were mainly aimed at quantifying inactivation rather than providing information on crucial aspects such as fluence rate and dose distribution, parameters known to govern reactor performance [20,21].

The impact of fluoropolymer UV absorption on disinfection has not been investigated to date, despite knowledge that the chemical composition and polymerization processes substantially affect the optical characteristics of the fluoropolymer and can ultimately

* Corresponding author.
E-mail address: dsantor@uwo.ca (D. Santoro).

1385-8947/$ – see front matter © 2010 Elsevier B.V. All rights reserved.
doi:10.1016/j.cej.2010.03.090

Nomenclature

a_λ	fraction of absorbed light at fixed wavelength
$C_{\varepsilon 1}$, $C_{\varepsilon 2}$, C_μ	turbulence model constants
D	UV dose [J m^{-2}]
d	sample thickness [m]
EEO	Electrical energy per order [W s m^{-3} log^{-1}]
I_λ	fluence rate at fixed wavelength [W m^{-2}]
k	fluence-based inactivation rate constant [m^2 J^{-1}]
N, N_0	residual or initial phage concentration [plaque ml^{-1}]
p	static pressure [kg m^{-1} s^{-2}]
P_k	production term in the turbulent kinetic energy equation [m^2 s^{-3}]
P_w	electrical lamp power [W]
Q	flowrate [m^3 s^{-1}]
r	position vector [m]
$r_{\lambda,\text{diffuse}}$	fraction of diffusely reflected light at fixed wavelength
Sc_t	turbulent Schmidt number
SS_i	sum of squares for the ith factor
SS_t	total sum of squares
S_ϕ	source term in the generalized convection–diffusion equation [Φ s^{-1}]
s'	scattering direction vector [m]
s	direction vector [m]
$t_{\lambda,\text{diffuse}}$	fraction of diffusely transmittance light
$t_{\lambda,\text{direct}}$	fraction of directly (regularly) transmittance light
$t_{\lambda,\text{total}}$	fraction of total transmittance light
$t_{\lambda,\text{total,trap}}$	fraction of total transmittance light with light trap at the reflectance port
UVT_{254}	UV transmittance at 254 nm [% cm^{-1}]
$-\overline{u_i' u_j'}$	Reynolds stress tensor components [m^2 s^{-2}]
$\{u, v, w\}$	velocity components [m s^{-1}]
$\{x, y, z\}$	Cartesian coordinates [m]

Greek letters

Γ_ϕ	diffusion coefficient in the generalized convection–diffusion equation [m^2 s^{-1}]
ε	turbulent dissipation rate [m^2 s^{-3}]
ε_λ	Naperian absorption coefficient at given wavelength [m^{-1}]
κ	turbulent kinetic energy [m^2 s^{-2}]
ν	kinematic viscosity [m^2 s^{-1}]
ν_t	turbulent kinematic viscosity [m^2 s^{-1}]
ρ	density [kg m^{-3}]
σ_ε,σ_κ	turbulent Prandtl numbers
$\sigma_{S,\lambda}$	scattering coefficient at given wavelength [m^{-1}]
Φ	general scalar [plaque ml^{-1}] or [W m^{-2}]
Ψ	phase function
Ω'	solid angle [steradian]

be expected to influence delivery of the reduction equivalent dose (RED). Funayama and Sugawara [22] conducted a comparative study on quartz and fluoropolymer tubes using chemical actinometry and demonstrated that a quartz tube has a higher transparency in the radiation band between 200 and 600 nm. They also reported a transmittance of 30% over a 0.25 mm thick fluoropolymer sample versus a 90% transmittance for a 1 mm thick quartz sample. Lowry et al. [23] documented an ultraviolet transmittance at 254 nm (UVT_{254}) of amorphous Teflon (AF) in the range of 70–75% for a 3.2 mm thick sample while Dever and McCracken [24] found a UVT_{254} of 55% for a Teflon FEP sample of 0.127 mm thickness. In a similar study, 50% UVT_{254} was observed on a 2 mm Teflon FEP sample [25]. Changes in optical properties were documented by Hougham et al. [26] as a result of fluoropolymer damage caused by absorbed photons with a reduction in transmitted light.

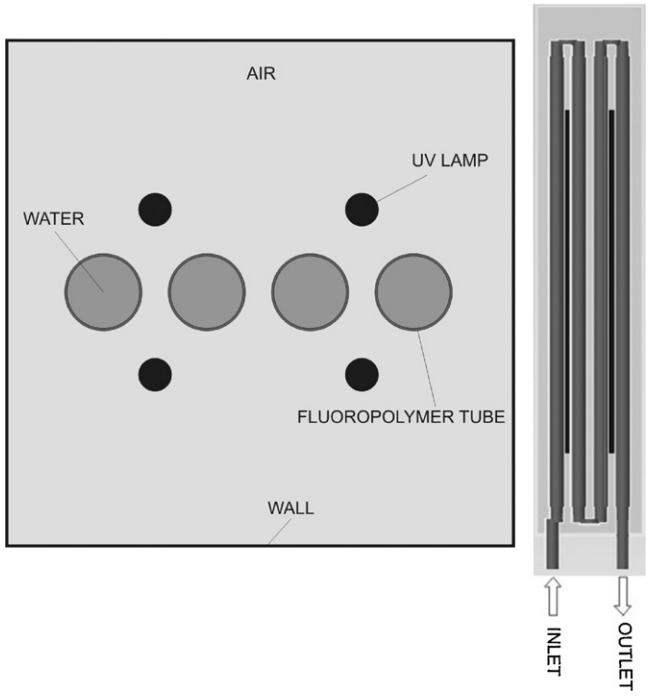

Fig. 1. Horizontal and vertical cross-sections of the fluoropolymer tube UV photoreactor.

Recently, Computational Fluid Dynamics (CFD) has emerged as a powerful technique to investigate and optimize water treatment processes and technologies such as sedimentation [27], disinfection [16,28,29] and advanced oxidation [30]. In this paper, the disinfection processes taking place in a pilot-scale fluoropolymer tube UV photoreactor were investigated using CFD. Flow, fluence rate, microbial inactivation and UV dose distribution were predicted in an Eulerian framework using the Fluent software (Ansys, Canonsburg) and compared against pilot biodosimetry data. Finally, critical factors affecting UV disinfection were identified via model sensitivity analysis and discussed in terms of potential impacts on short and long term disinfection efficiency and operational cost.

2. Materials and methods

2.1. Fluoropolymer tube photoreactor

The pilot photoreactor is composed of four fluorinated ethylene propylene (FEP) tubes (also known as fluoropolymer tubes or Teflon tubes) having an outer diameter of 35 mm and a thickness of 1.2 mm (Fig. 1). Four monochromatic low pressure UV lamps (253.7 nm, 39 W electrical power, 40% nominal lamp efficiency) are mounted parallel to the tubes and enclosed in a 250 mm × 250 mm × 1200 mm stainless steel cabinet. When in operation, the system is cooled by forced ventilation through a fan installed at the cabinet wall.

The fluid enters the reactor at a variable volume flowrate in the range of 0.84–1.51 l s^{-1} (Re = 30,420–54,685) from the bottom (inlet) and moves in a serpentine fashion while being continuously exposed to the fluence rate field. The plastic elbows that connect the four fluoropolymer tubes are made of polyvinyl chloride. Thus, they are opaque to the UV radiation. After UV disinfection, the fluid exits the reactor from an outlet located in proximity to the reactor inlet.

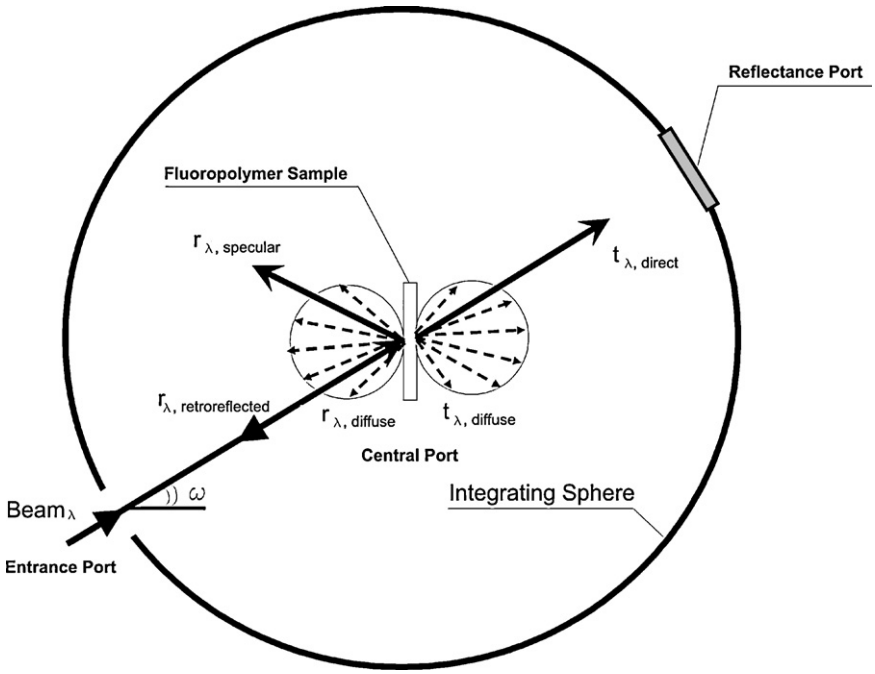

Fig. 2. Relevant light components in an integrating sphere apparatus.

2.2. Optical measurements

Because fluoropolymers are known to significantly scatter UV light [31], all optical measurements were carried out using a Cary100 spectrophotometer (Varian, Walnut Creek, USA) equipped with the integrating sphere accessory (Labsphere, North Sutton, USA). As schematically illustrated in Fig. 2, the interaction between the light beam and a highly scattering material will result in multiple light components [32]. When the angle of incidence between the beam and the sample is orthogonal ($\omega = 0$), the retro-reflected ($r_{\lambda,\text{retro-reflected}}$) and the specularly reflected ($r_{\lambda,\text{specular}}$) components are excluded from the transmittance measurement. Using this configuration, two types of transmittance measurements can be taken.

If a purely reflective standard (Spectralon USRS-99-020) is placed at the reflectance port, total transmittance measured by the integrating sphere spectrophotometer will be:

$$t_{\lambda,\text{total}} = t_{\lambda,\text{direct}} + t_{\lambda,\text{diffuse}} + r_{\lambda,\text{diffuse}} \quad (1)$$

where $t_{\lambda,\text{direct}}$, $t_{\lambda,\text{diffuse}}$ and $r_{\lambda,\text{diffuse}}$ are the contributions to the total transmittance measurement from the directly transmitted, diffusely transmitted, and diffusely reflected light, respectively. Similarly, if a light trap is placed at the reflectance port to exclude from the measurement the contribution of the directly transmitted component, total transmittance will be:

$$t_{\lambda,\text{total,trap}} = t_{\lambda,\text{diffuse}} + r_{\lambda,\text{diffuse}} \quad (2)$$

Thus, by taking the difference between the two previously described measurements, the direct component ($t_{\lambda,\text{direct}}$) of the transmitted light can be estimated:

$$t_{\lambda,\text{direct}} = t_{\lambda,\text{total}} - t_{\lambda,\text{total,trap}} \quad (3)$$

and the fraction of absorbed light accordingly calculated (Eq. (4)):

$$a_\lambda = 1 - (t_{\lambda,\text{total}}) \quad (4)$$

Finally, a Beer–Lambert-equivalent Naperian fluoropolymer absorption coefficient (ε_λ) can be estimated and used for CFD simulations to model the energy losses occurring in the fluoropolymer tubes exposed to UV light, as in Eq. (5):

$$\varepsilon_\lambda = \frac{1}{d} \ln\left[\frac{1}{1 - a_\lambda}\right] \quad (5)$$

where d is the fluoropolymer sample thickness.

Table 1
Values of Φ, Γ_Φ and S_Φ for the convection and diffusion equation in Cartesian coordinate system.

#	Equation	Φ	Γ_Φ	S_Φ
a	Continuity	1	0	0
b	Momentum in x direction	u	$\nu + \nu_t$	$-\frac{1}{\rho}\frac{\partial(p+2k/3)}{\partial x}$
c	Momentum in y direction	v	$\nu + \nu_t$	$-\frac{1}{\rho}\frac{\partial(p+2k/3)}{\partial y}$
d	Momentum in z direction	w	$\nu + \nu_t$	$-\frac{1}{\rho}\frac{\partial(p+2k/3)}{\partial z}$
e	Turbulent kinetic energy	k	$\nu + \frac{\nu_t}{\sigma_k}$	$P_k - \varepsilon$
f	Dissipation rate	ε	$\nu + \frac{\nu_t}{\sigma_\varepsilon}$	$C_{\varepsilon 1}\frac{\varepsilon}{k}P_k - C_{\varepsilon 2}\frac{\varepsilon^2}{k}$
g	Scalar (microbial inactivation)	N	$\frac{\nu_t}{Sc_t}$	$-klN$
h	Scalar (UV dose)	D	0	$+I$

2.3. Mathematical modeling: governing equations

The detailed mathematical formulation of the problem under investigation is provided below. For an incompressible Newtonian flow, the time-averaged governing equations of mass, momentum, turbulence parameters, microbial inactivation and UV dose can be written using the generalized form of the convection–diffusion equation (Eq. (6)):

$$\frac{\partial u\phi}{\partial x} + \frac{\partial v\phi}{\partial y} + \frac{\partial w\phi}{\partial z} = \frac{\partial}{\partial x}\left[\Gamma_\phi \frac{\partial \phi}{\partial x}\right] + \frac{\partial}{\partial y}\left[\Gamma_\phi \frac{\partial \phi}{\partial y}\right] + \frac{\partial}{\partial z}\left[\Gamma_\phi \frac{\partial \phi}{\partial z}\right] + S_\phi \quad (6)$$

where the values of Φ, Γ_Φ and S_Φ are given in Table 1.

The standard k–ε model with wall functions was used in this study due to its ability to provide a reasonable description of fully turbulent flows. While it has been conclusively demonstrated that such a model is inadequate to describe flows dominated by vortex shedding or swirling [33], good performance was documented by Sozzi and Taghipour [34] in predicting velocity profiles obtained

Table 2
Empirical constants for the k–ε model [37].

$C_{\varepsilon 1}$	$C_{\varepsilon 2}$	C_μ	σ_κ	σ_ε
1.44	1.92	0.09	1.0	1.3

from particle image velocimetry (PIV) experiments in L-shape and U-shape photoreactors.

The mathematical derivation of this model is reported in detail elsewhere [35]. The standard k–ε model is a semi-empirical model based on model transport equations for the turbulence kinetic energy k and its dissipation rate ε. In these equations, P_k represents the generation of turbulence kinetic energy due to the mean velocity gradients. This term is defined as:

$$P_k = -\overline{u_i' u_j'} \frac{\partial u_j}{\partial x_i} \tag{7}$$

where $-\overline{u_i' u_j'}$ are the Reynolds stress tensor components which can be related to the mean velocity gradient using the Boussinesq hypothesis [36]. The model constants $C_{\varepsilon 1}$, $C_{\varepsilon 2}$, C_μ, σ_κ and σ_ε used in this study are summarized in Table 2.

The concentration of surviving microbes and UV dose was predicted by solving two additional scalar transport equations (Table 1, equations g and h). The source term of the microbial transport equation represents a first order kinetic in both fluence rate and microbial concentration. While the fluence-based microbial inactivation rate constants were determined through collimated beam experiments, the source term in the UV dose scalar transport equation was set equal to the local fluence rate value. This way, the accumulated dose as a function of the fluid trajectory can be predicted in an Eulerian framework as long as the turbulent diffusion term is removed from the transport equations [20]. If, instead, such a term was left in the computation, the Eulerian and Lagrangian dose distributions could substantially differ [45]. Therefore, the scalar diffusion coefficient of the UV dose transport equation was set to zero.

Furthermore, the scalar diffusion coefficient for the microbial transport equation was also set to zero, in consideration that: (a) no gradients in microbial concentration are generated during the UV treatment (e.g., microbes are not removed from the system), (b) nanosized particles such as MS2 and T1 coliphages have a very low diffusivity in water at 20 °C, in the order of 10^{-10} to 10^{-11} m^2 s^{-1} [38] and (c) while the elbows are the regions promoting highest turbulent diffusion, they are also opaque to the ultraviolet radiation hence the fluid is not exposed to the fluence rate field in that portion of the photoreactor (the UV dose distribution remains unchanged).

Nevertheless, to further validate these assumptions, four sets of CFD simulations (at low and high RED doses) were carried out and compared: the first set of simulated microbial inactivation is obtained using a diffusion coefficient of zero, while the remaining are accounting for the contribution of the turbulent viscosity throughout the reactor for turbulent Schmidt numbers varying from 0.5 to 1.5 (Table 3). As can be seen, inclusion of turbulent diffusion has a negligible impact on microbial inactivation thus confirming that convection is the dominant transport mechanism occurring in the photoreactor for the investigated Re numbers (Re = 30420–54685).

2.4. Fluence rate model

The derivation of the radiative transport equation (RTE) is well established [39]. The Fluent DO model solves the RTE using a directional and spatial discretization around the radiation source. On each computational cell, a local radiation balance is carried out by solving the partial integro-differential equation (Eq. (8)):

$$\frac{dI_\lambda(s_i)}{dx_i} + (\varepsilon_\lambda + \sigma_{S,\lambda}) I_\lambda(r,s) = \frac{\sigma_{S,\lambda}}{4\pi} \int_0^{4\pi} I_\lambda(r,s') \Psi(s \cdot s') d\Omega' \tag{8}$$

In our problem, such equation should be simultaneously solved for the three adjacent media, namely air, fluoropolymer and water, using the appropriate initial and boundary conditions.

While scattering of UV light can be neglected in both water and air, such phenomenon represents the main mechanism for UV propagation in fluoropolymers [31], as also confirmed by the measurements taken in this study on the fluoropolymer transmittance (Fig. 4). Thus, appropriate boundary conditions were assigned to both the semi-transparent walls to ensure that the light transmitted across the fluoropolymer tubes was diffusely and isotropically re-emitted in the fluid region. The approach used in this study to model fluoropolymer scattering through the use of a semi-transparent wall boundary condition allowed a further simplification of the RTE since the fluoropolymer scattering coefficient could now be set to zero (Eq. (9)):

$$\frac{dI_\lambda(s_i)}{dx_i} + \varepsilon_\lambda I_\lambda(r,s) = 0 \tag{9}$$

where x_i and s_i are position and direction vectors, respectively, and ε_λ is the wavelength-dependent absorption coefficient of the three media (air, fluoropolymer tube, water).

2.5. Computational Fluid Dynamics (CFD) model

2.5.1. Model setup

All simulations were carried out in an Eulerian framework using the Fluent software (Ansys, Canonsburg, USA). A 3D mesh with 437,789 cells was generated in Gambit software by extruding a horizontal 2D grid (identified via mesh independence studies) in the third vertical dimension. The remaining parts of the computation domain (i.e., the fluoropolymer tube connections and the inlet-outlet piping) were meshed using an unstructured tetrahedral grid.

A velocity inlet boundary condition was imposed to prescribe the desired flowrates, while a pressure outlet boundary condition was applied at the reactor exit.

The discrete ordinates (DO) radiation model was employed to solve the RTE in the computational domain using as a solid angle discretization, with a theta and phi division of 7 and 3, respectively. Due to the relatively small thickness (1.2 mm) and the dominant mechanism of light propagation across the fluoropolymer tube, a diffuse fraction of 1 was assigned to the semi-transparent walls separating the tubes from the surrounding environment (air and water).

Table 3
Impact of the diffusion coefficient Γ_ϕ on predicted T1 and MS2-RED [mJ cm^{-2}] for different turbulent Schmidt numbers at high and low UV doses.

	$\Gamma_\phi = 0$	$\Gamma_\phi = \nu_t/(Sc_t = 0.5)$	$\Gamma_\phi = \nu_t/(Sc_t = 0.9)$	$\Gamma_\phi = \nu_t/(Sc_t = 1.5)$
Q = 1.51 l s^{-1} UVT = 56.8% cm^{-1} [low UV dose]	MS2-RED = 20.08 T1-RED = 18.32	MS2-RED = 20.32 T1-RED = 18.55	MS2-RED = 20.21 T1-RED = 18.46	MS2-RED = 20.12 T1-RED = 18.36
Q = 0.84 l s^{-1} UVT = 77.8% cm^{-1} [high UV dose]	MS2-RED = 57.63 T1-RED = 50.6	MS2-RED = 58.88 T1-RED = 51.77	MS2-RED = 58.51 T1-RED = 51.42	MS2-RED = 58.20 T1-RED = 51.12

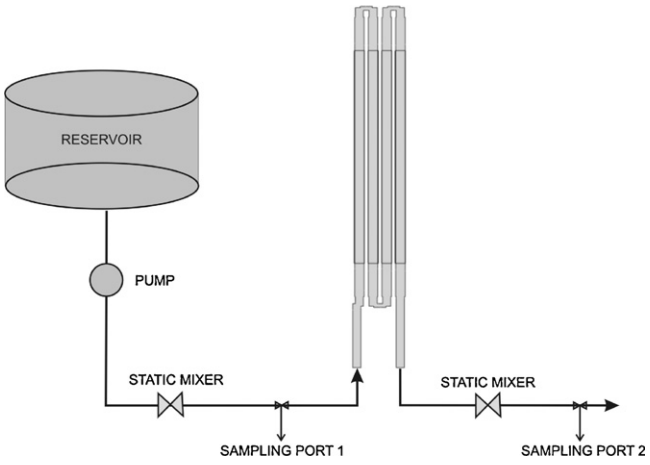

Fig. 3. System layout used for biodosimetry experiments.

The amount of reflection and absorption of the stainless steel cabinet was determined by inferring the diffuse fraction and the emissivity of the cabinet walls using numerical optimization. Specifically, the Simplex algorithm was used in conjunction with automated CFD simulations to minimize the error between observed and simulated MS2 and T1 inactivation.

A second order accurate upwind discretization scheme was employed to approximate the nonlinear convective terms in all governing equations while the SIMPLE (Semi-Implicit Method for Pressure-Linked Equations) algorithm was employed for pressure correction [40].

2.5.2. Model calibration

Bioassay tests, conducted according to the EPA guidance manual [41], were performed in order to collect data to be used for CFD calibration. A 1000 l tank filled with dechlorinated tap water was spiked with MS2 and T1 to give an initial virus density of 2.6×10^5 pfu ml^{-1} and 2.6×10^6 pfu ml^{-1}, respectively, and continuously mixed using a submersible pump. The UVT_{254} of the water was modified by adding a suitable amount of soluble coffee to the water and the reactor flowrate was adjusted using a valve located at the reactor outlet. Static mixers were installed both at the inlet and outlet of the reactor and immediately before and after the sampling ports to ensure that the collected water samples were representative of the delivered UV treatment (Fig. 3).

Inactivation experiments were conducted under nine different test conditions resulting from the factorial combinations of three UVT_{254} values (58.6, 67.9, 77.8% cm^{-1}) and three flowrates (0.84, 1.26, 1.51 l s^{-1}). Two samples for collimated beam testing were withdrawn from the system at the beginning and the end of the bioassay experiments and irradiated at known UV doses to determine the dose–response curves (and thus the inactivation rate constant for both MS2 and T1 bacteriophages) and to confirm that the fluid mixture was stable throughout the experiments. After reaching pseudo steady-state condition and for each test point, triplicate inlet and outlet samples were collected in order to quantify surviving bacteriophages and delivered UV dose. Bacteriophages were enumerated according to the protocol described in Appendix A of the EPA UV Disinfection Design Guidance Manual [41].

Special attention was paid to the fluence rate model calibration. First, a model sensitivity study was carried out using a 2-level full-factorial scheme. Screened factors included the fluoropolymer absorption coefficient, the scattering coefficient, the water UVT_{254}, the lamp power, the wall emissivity and the diffuse fraction. For factors responsible for >1% of the total variability (as sum of square) described by the CFD model, their values were experimentally determined or inferred using the Simplex algorithm [42]. From a geometrical viewpoint, the simplex methods correspond to a polyhedron containing $N+1$ points in a N dimensional space (e.g., a triangle in a two dimensional optimization problem). These points are moved according to three possible operations: reflection, expansion and contraction [43]. Their movement is driven by the objective function, defined in this study as the square root of the squared sum of error between observed and simulated MS2-RED over the entire range of flowrates and UVT. The algorithm terminates when a solution with improvements greater than the assigned tolerance (set in this work to 0.1 mJ/cm^2 MS2-RED) cannot be found.

The non-significant factors were treated as constants and default values derived from previous studies were assigned.

3. Results and discussion

3.1. Fluoropolymer absorption spectrum

The wavelength-dependent fluoropolymer transmittance spectra, measured using an integrating sphere spectrophotometer, are shown in Fig. 4. In one case, a light trap was installed at the reflectance port to exclude the direct component of transmitted light from the measurement. As expected, the lowest wavelengths (<220 nm) are strongly attenuated by the fluoropolymer material.

As can be noted in Fig. 4, the contribution of the direct component, given by the difference between the two curves, is almost negligible for wavelengths lower than 260 nm. This further validates the hypothesis that, at 254 nm, the light propagation across the fluoropolymer tubes mainly occurs through scattering events resulting into a diffuse transmittance of UV light. At 254 nm, the percent of absorbed energy was equal to 13.5%, giving a Beer–Lambert equivalent Naperian absorption coefficient of 120.9 m^{-1}. Such value has been used for the CFD simulations to model the energy losses occurring in the fluoropolymer tube thickness.

3.2. CFD simulations

3.2.1. Grid independence studies

Grid independence studies were carried out on a representative 2D cross-section of the UV photoreactor to determine the mini-

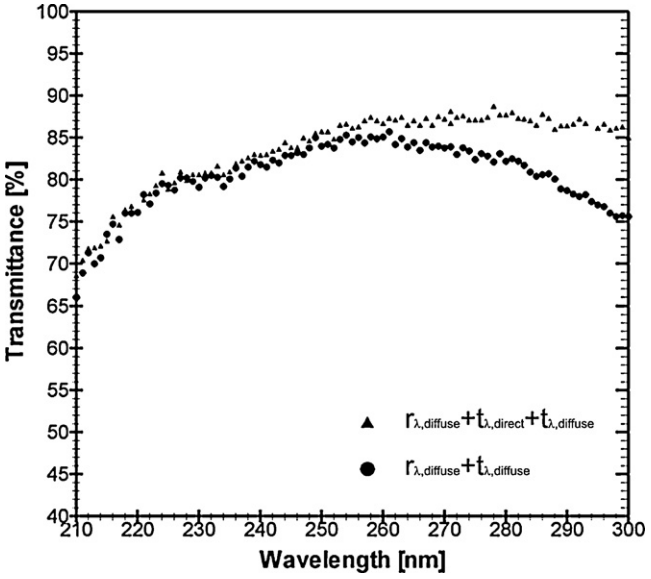

Fig. 4. Transmittance spectra of the fluoropolymer tube (1.2 mm thick sample).

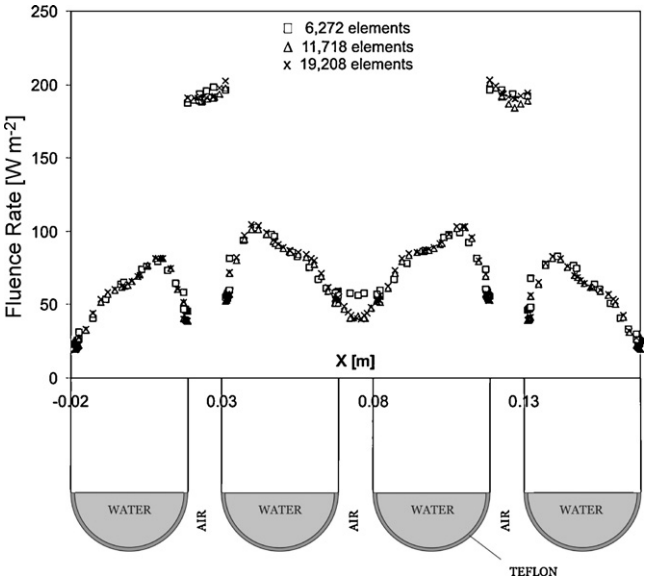

Fig. 5. Fluence rate profiles for three different computational grids.

mum number of elements needed to accurately solve the RTE and obtain the fluence rate distribution. Fig. 5 shows the fluence rate profile across three reactor zones, namely the air, the fluoropolymer tube and the water, for a horizontal reactor cross-section. As can be noted, the fluence rate profile becomes mesh-independent for grids with a number of cells greater than 11,718.

3.2.2. Model sensitivity analysis

A model sensitivity analysis has been conducted according to a full-factorial two level design of experiment using MS2 log inactivation as response variable. For a critical parameter such as the lamp power, the range of variation has been determined based on information provided by the manufacturer on the peak UV efficiency (40% at $T = 40\,^{\circ}C$) and the potentially severe depletion and instability in the UV output due to operation at non-optimal temperatures. Similarly, the low end-of-range for the fluoropolymer absorption coefficient has been set to zero in consideration that new fluoropolymer materials with lower UV_{254} absorption are likely to be developed and, in spite of their fragility, quartz tubes could also be used for UV applications involving non-pressurized fluids.

The percent of contribution (PC) on total variability described by the CFD model can be estimated using Eq. (10):

$$PC(\%) = 100 \times \frac{SS_i}{SS_t} \tag{10}$$

where SS_i is the sum of squares of ith factor and SS_t is the total sum of squares of the CFD model in the investigated range of factors. Table 4 summarizes the range of variability and the percentage of contribution of each factor on the simulated log inactivation.

Over a total sum of squares of 23.3, three key factors such as fluoropolymer absorption coefficient, lamp power, and UV reflection at the cabinet walls (i.e., the cabinet wall emissivity and diffuse fractions) were responsible for >85% of the simulated log inactivation. The remaining factors such as diffuse fractions at the semi-transparent tube interfaces were able to explain only 0.3% while the sum of the percent of contribution for all higher order interactions were responsible for less than 3.3% of SS_t.

3.2.3. Model calibration

While the fluoropolymer absorption coefficient was experimentally determined, the remaining significant factors were inferred using an optimization algorithm (Simplex) and automated CFD simulations. The computational search was conducted by exploring the space of parameters used for model sensitivity analysis. Notably, the calibrated value for the total reflected light (~30%) at the stainless steel cabinet wall was in good agreement with published information on stainless steel reflection at 254 nm (~25% as in Koller [44]). Likewise, the lamp power value identified via numerical optimization returned a lamp efficiency that was consistent with the one provided by the manufacturer (Table 5).

The MS2 and T1 dose–response curves, determined using a collimated beam apparatus, are shown in Fig. 6. As expected, T1 was found to be more sensitive-to-UV light than MS2 in agreement with previous studies [45]. As can be seen, MS2 and T1 inactivation kinetics were well described by a first order kinetic model with decadic fluence-based rate constants of 0.047 $cm^2\,mJ^{-1}$ and 0.200 $cm^2\,mJ^{-1}$, respectively. Such constants were used in the Eulerian CFD model to predict the bacteriophage transport and inactivation in the fluoropolymer photoreactor.

Figs. 7 and 8 show the observed MS2 and T1-RED and the CFD predicted RED values calculated using the dose–response curve from collimated beam experiments. Overall, the CFD model accurately describes the observed trends and log removal for both bacteriophages over the entire range of UVT_{254}'s and flowrates. However, the model tends to overpredict T1 disinfection at higher UV doses (>20 $mJ\,cm^{-2}$) which may be explained by an overestimation of the rate of inactivation due to model extrapolations occurring at such doses where the T1 dose–response curve was not measured (Fig. 6) and microbial clumping and tailing may have occurred.

Other possible reasons of such discrepancy may be found in the inability of the turbulence model and the steady-state assumption

Table 4
Model sensitivity analysis: analysis of variance (partial sum of squares).

Parameter	Unit	Range	*SS*	PC (%)	Decision
Fluoropolymer absorption coefficient	m^{-1}	0–1000	15.31	65.69	Significant
Lamp power	W	7.8–15.7	2.80	12.04	Significant
Cabinet wall emissivity	–	0–1	1.01	4.31	Significant
Cabinet wall diffuse fraction	–	0–1	0.90	3.86	Significant
Diffuse fraction (air–tube interface)	–	0–1	0.066	0.28	Not significant
Diffuse fraction (tube–water interface)	–	0–1	3.66×10^{-3}	0.016	Not significant

Table 5
Significant optical parameters and their adopted values in the CFD model.

Parameters	Optimal value	Determination technique
Fluoropolymer absorption coefficient	120.9 m^{-1}	Measured
Lamp UV power	15.7 W	Inferred
Stainless steel wall emissivity	0.79	Inferred
Stainless steel wall diffuse fraction	0.85	Inferred

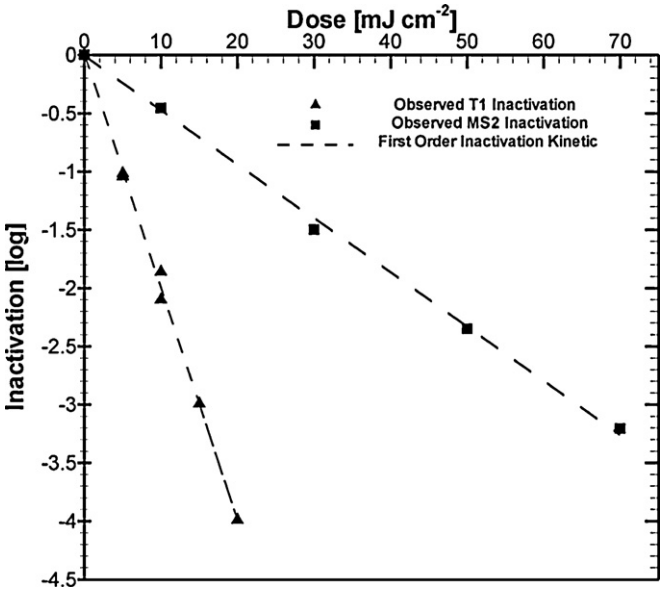

Fig. 6. Dose–response curve for MS2 and T1.

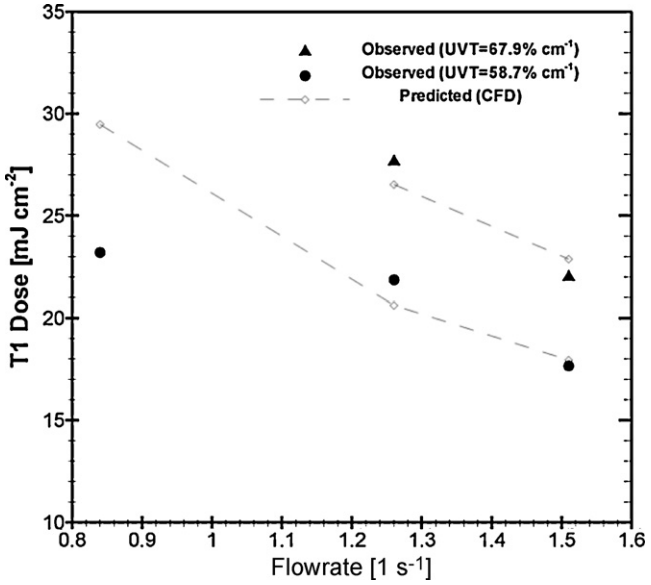

Fig. 8. Comparison between observed and predicted T1-RED.

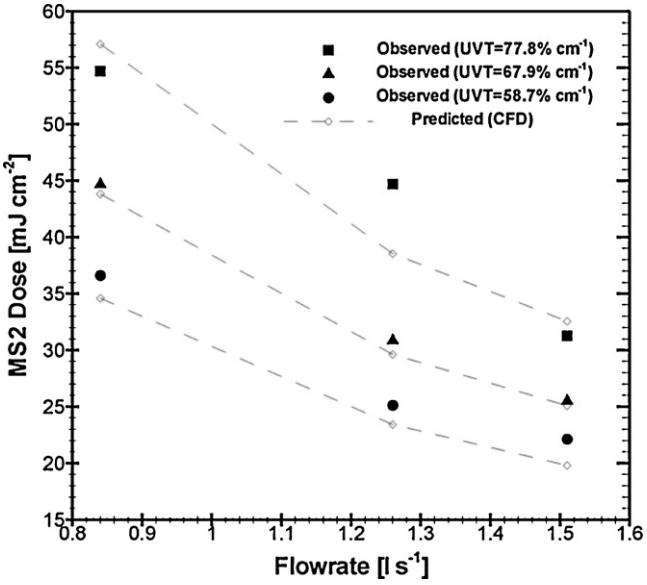

Fig. 7. Comparison between observed and predicted MS2-RED.

employed in this study to predict the intensity of three-dimensional vortex occurring in the photoreactor. Such secondary flows may determine poor predictions of the low-end values of the UV dose distribution, which is a region known to govern the observed performance when sensitive-to-UV microbes such as T1 are employed for bioassay experiments.

3.2.4. Spatial distributions

Velocity magnitude and velocity vectors were computed and are displayed in Fig. 9 for a flowrate of 1.261 s^{-1}. As the vector plot reveals, plug flow conditions occur in the fluoropolymer tubes while considerable mixing is promoted by separation and recirculation at the narrow plastic 180° bends employed to connect the four fluoropolymer tubes in series.

The predicted fluence rate and dose distributions are displayed in Fig. 10. As expected, while higher fluence rate regions are predicted in close proximity to the UV lamps (air region), a considerable drop in fluence rate occurs inside the fluoropolymer tubes, due to both absorption and scattering events occurring in the fluoropolymer tube and the water. Nevertheless, while a considerable fluence rate gradient is displayed in each tube (Fig. 5), the average fluence rate appears to be similarly distributed among the four fluoropolymer tubes in a horizontal cross-section. As a result of both the serpentine trajectories and fluence rate distribution, the delivered UV dose increases almost linearly along the main flow path (Fig. 10).

Table 6
Simulated and observed MS2 [T1] log inactivation at different test conditions.

		Log N_0/N [Abs. coeff. = 60 m^{-1}] CFD model	Log N_0/N [Abs. coeff. = 120 m^{-1}] CFD model	Log $N_0/N \pm$ St. Dev. [Abs. coeff. = 120 m^{-1}] Experimental	Log N_0/N [Abs. coeff. = 180 m^{-1}] CFD model
Flow = 0.841 s^{-1}	UVT_{254} = 77.8% cm^{-1}	3.1 [11.1]	2.7 [10.1]	2.6 ± 0.13 [n/a]	2.4 [9.1]
	UVT_{254} = 67.9% cm^{-1}	2.3 [8.9]	2.1 [7.3]	2.1 ± 0.21 [n/a]	1.9 [6.3]
	UVT_{254} = 58.6% cm^{-1}	1.8 [6.7]	1.6 [5.9]	1.7 ± 0.17 [4.6 ± 0.03]	1.5 [5.4]
Flow = 1.261 s^{-1}	UVT_{254} = 77.8% cm^{-1}	2.1 [8.0]	1.8 [7.0]	2.1 ± 0.20 [n/a]	1.6 [6.2]
	UVT_{254} = 67.9% cm^{-1}	1.6 [5.9]	1.4 [5.3]	1.5 ± 0.15 [5.5 ± 0.2]	1.3 [4.8]
	UVT_{254} = 58.6% cm^{-1}	1.2 [4.5]	1.1 [4.1]	1.2 ± 0.07 [4.4 ± 0.05]	1.0 [3.8]
Flow = 1.511 s^{-1}	UVT_{254} = 77.8% cm^{-1}	1.8 [6.6]	1.5 [6.0]	1.5 ± 0.16 [n/a]	1.4 [5.3]
	UVT_{254} = 67.9% cm^{-1}	1.3 [4.6]	1.2 [4.6]	1.2 ± 0.18 [4.4 ± 0.21]	1.1 [4.1]
	UVT_{254} = 58.6% cm^{-1}	1.0 [4.0]	0.9 [3.6]	1.0 ± 0.04 [3.5 ± 0.06]	0.8 [3.3]

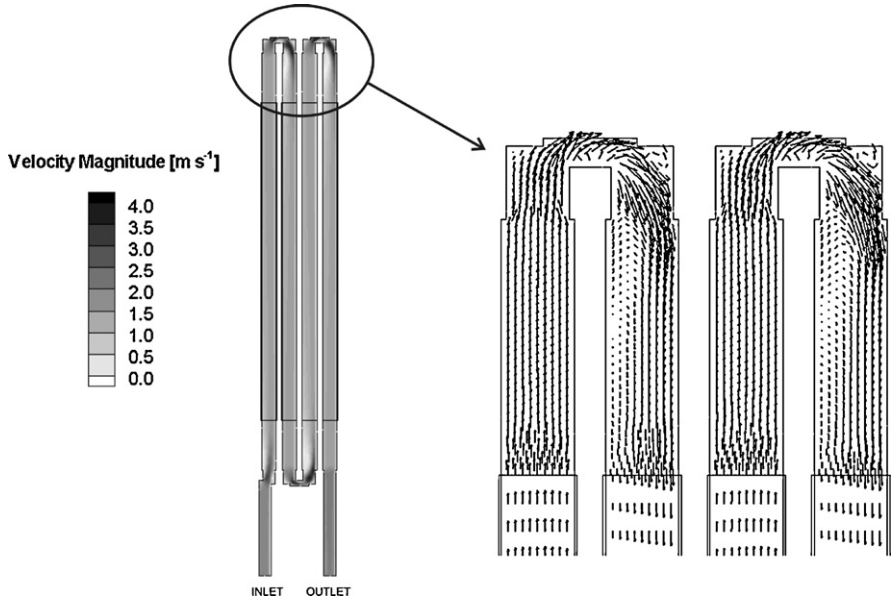

Fig. 9. Velocity magnitude (left) and zoomed velocity vectors (right) of the photoreactor.

3.2.5. Fluoropolymer purity and reactor performance

The critical role of fluoropolymer UV absorption on reactor performance was assessed using the calibrated CFD model for three different scenarios. In one case (Abs. coeff. = 120 m^{-1}), both modeling and experimental were available while, for the remaining two cases (Abs. coeff. = 60 and 180 m^{-1}), the impact on reactor performance was only assessed numerically. Results are summarized in Table 6.

As expected, for both MS2 and T1, a linear drop in disinfection performance (in the range of 9–11%) occurred when the fluoropolymer absorption coefficient increased by 33%. For each scenario, the specific energy consumption was also estimated using Eq. (11):

$$\mathrm{EEO} = \frac{P_w}{Q \log N_0/N} \tag{11}$$

where N_0 is the phage concentration at the reactor inlet [pfu ml^{-1}], N is the phage concentration at the reactor outlet [pfu ml^{-1}], P_w is the electrical power of the UV lamps [kW] and Q is the flowrate [m^3 s^{-1}]. Results, summarized in Table 7, are compared against data from previous studies on conventional UV photoreactors [20,46].

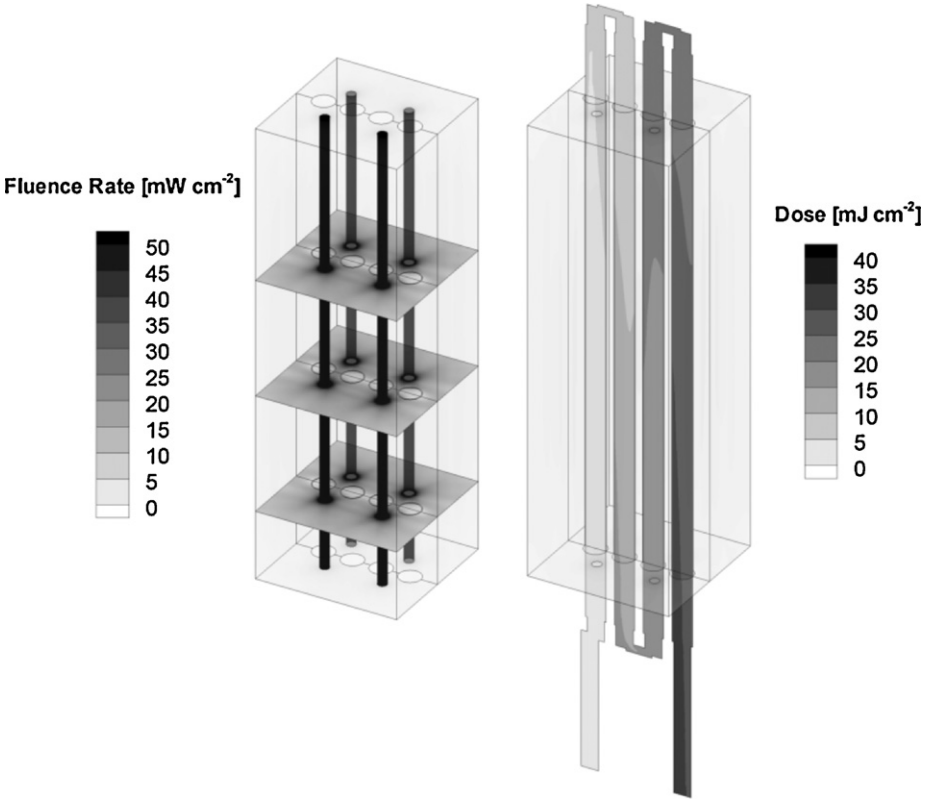

Fig. 10. Fluence rate (right) and cumulated UV dose (left) in the fluoropolymer UV photoreactor (flowrate = 1.26 l s^{-1}, UVT_{254} = 67.9% cm^{-1}).

Table 7
Electrical energy per log inactivation of MS2 [kWh m^{-3} log^{-1}] at different UVT_{254}.

	This study (2010) (fluoropolymer)	Sozzi and Taghipour [46] (quartz)	Ducoste et al. [20] (quartz)
UVT_{254} = 77.8% cm^{-1}	0.0190	n/a	0.0049
UVT_{254} = 67.9% cm^{-1}	0.0241	0.0044	n/a
UVT_{254} = 58.6% cm^{-1}	0.0289	n/a	n/a

As shown in Table 7, a substantial increase of the EEO (in the range of 3.9–5.5 times) was observed if the investigated photoreactor (fluoropolymer tube absorption coefficient = 120.9 m^{-1}) is compared to conventional UV technologies [20,46]. Such inefficiency results from the combination of at least three negative effects: (a) a reduced amount of photons reaching the fluid due to the relatively narrow view-angle between the fluoropolymer tubes and the UV lamps; (b) a considerable loss of photons occurring in the fluoropolymer tubes due to absorption events; (c) a relatively small contribution of reflection (~30%) at the stainless steel walls.

This may suggest that the investigated technology may not be ideal for high-flow installations or applications where the energy efficiency is a concern. Nevertheless, further research is required to investigate whether such inefficiency can be minimized, for example, by employing internal UV reflectors, new UV-transparent materials and reactor shape optimization.

4. Conclusions

Based on the outcome of this study, the following conclusions can be made:

- The CFD model predicted reasonably well the disinfection performance of the external-lamp fluoropolymer tube photoreactor across the entire range of test conditions, with an error ranging from −13.7% to +4.4% for MS2 (average = −3.9%) and from −5.6% to +27.0% for T1 (average = +4.6%) thus indicating that delivered UV dose of such systems can be estimated using a numerical approach.
- The calibrated CFD model enables one to visualize simultaneously the fluence rate, the UV dose, the MS2 and T1 distributions in the photoreactor and hence, ultimately to gather accurate, spatially dependent information on UV reactor performance.
- Model sensitivity studies revealed that the fluoropolymer UV absorption has a considerable impact on photoreactor performance. Such evidence is also supported by measurements on the fluoropolymer transmittance spectra which indicated that the percentage of energy absorbed at 254 nm by a 1.2 mm thick tube can be as high as 13.5%.
- Under the test conditions used, the electrical energy per log of MS2 inactivation of the fluoropolymer tube photoreactor was as high as 0.019–0.029 kWh m^{-3} MS2 log^{-1} which is higher than conventional UV reactors (0.0044–0.0049 kWh m^{-3} MS2 log^{-1}), indicating that such systems may not be ideal for energy sensitive applications.

Acknowledgements

This research has been supported (in part) through the Exploratory Grant # 021 “CFD Simulation and Multi-objective Optimization as Supporting Tools for Advanced Water Treatment Plant Design”, funded by the Puglia Region (Italy). Special thanks are due to the industrial sponsors (G.nni Putignano & Figli SrL - Noci, IT and Novus SrL - Brindisi, IT) as well as to Trojan Technologies (London, Ontario, Canada), Dr. Mehrdad Raisee (University of Teheran) and Dr. Tiziano Pastore (Technical University of Bari) for the technical assistance and support provided throughout the investigation.

References

[1] P.C. Singer, Complying with trihalomethane reduction requirements in water treatment facilities, Pollution Technology Review 167 (1989).
[2] M.J. Rodriguez, J.B. Sérodes, P. Levallois, F. Proulx, Chlorinated disinfection by-products in drinking water according to source, treatment, season, and distribution location, Journal of Environmental Engineering Science 6 (2007) 355–365.
[3] G. Tchobanoglous, F.L. Burton, H.D. Stensel, Wastewater Engineering: Treatment and Reuse, McGraw-Hill, 2005.
[4] L.Y.C. Leon, J. Kuo, C.C. Tang, Disinfection of Wastewater Effluent: Comparison of Alternative Technologies, WERF, 2008.
[5] A. Downes, T.P. Blunt, Researches on the effect of light upon bacteria and other organisms, Proceedings of the Royal Society of London 26 (1877).
[6] G.O. Schenck, Ultraviolet Sterilization, Handbook of Water Purification, Ellis Horwood Ltd., Chichester, 1981, pp. 530–595.
[7] J.C. Chang, S.F. Ossoff, D.C. Lobe, M.H. Dorfman, C.M. Dumais, R.G. Qualls, J.D. Johnson, UV Inactivation of pathogenic and indicator microorganisms, Applied and Environmental Microbiology 49 (1985) 1361–1365.
[8] R.G. Qualls, D.J. Johnson, Bioassay and dose measurement in UV disinfection, Applied and Environmental Microbiology 45 (1983) 872–877.
[9] A.M. Shaban, G.E. El-Taweel, G.H. Ali, UV ability to inactivate microorganisms combined with factors affecting radiation, Water Science and Technology 35 (1997) 107–112.
[10] M.L. Janex, P. Savoye, Z. Do-Quang, E.R. Blatchley III, J.M. Laine, Impact of water quality and reactor hydrodynamics on wastewater disinfection by UV, use of CFD modelling for performance optimization, Water Science and Technology 38 (1998) 71–78.
[11] E.R. Blatchley III, Numerical modelling of UV intensity: application to collimated-beam reactors and continuous-flow system, Water Research 31 (1997) 2205–2218.
[12] J.J. Ducoste, K. Linden, Determination of ultraviolet sensor location for sensor set-point monitoring using computational fluid dynamics, Journal of Environmental Engineering and Science 4 (2005) 33–43.
[13] L. Liberti, M. Notarnicola, G. Boghetich, A. Lopez, Advanced treatment for municipal wastewater reuse in agriculture. UV disinfection: bacteria inactivation, Journal of Water Services Research and Technology—Aqua 50 (2001) 275–285.
[14] D. Liu, C. Wu, K. Linden, J.J. Ducoste, Numerical simulation of UV disinfection reactors: evaluation of alternative turbulence models, Applied Mathematical Modelling 31 (2007) 1753–1769.
[15] D.A. Lyn, K. Chiu, E.R. Blatchley III, Numerical modeling of flow and disinfection in UV disinfection channels, Journal of Environmental Engineering 125 (1999) 17–26.
[16] S. Elyasi, F. Taghipour, Simulation of UV photoreactor for water disinfection in Eulerian framework, Chemical Engineering Science 61 (2006) 4741–4749.
[17] T. Koutchma, B. Parisi, S. Unluturk, Evaluation of UV dose in flow-through reactors for fresh apple juice and cider, Chemical Engineering Communications 193 (2006) 715–728.
[18] V. Pareek, S. Chong, M. Tadé, A.A. Adesina, Light intensity distribution in heterogenous photocatalytic reactors, Asia-Pacific Journal of Chemical Engineering 3 (2008) 171–201.
[19] H. Muller-Steinhagen, Heat Exchanger Fouling and Cleaning: Fundamentals and Applications, Institution of Chemical Engineers, 2000.
[20] J.J. Ducoste, D. Liu, K. Linden, Alternative approaches to modeling fluence distribution and microbial inactivation in ultraviolet reactors: Lagrangian versus Eulerian, Journal of Environmental Engineering 131 (2005) 1393–1403.
[21] E.R. Blatchley III, C. Shen, Z. Naunovic, L.S. Lin, D.A. Lyn, J.P. Robinson, K. Ragheb, G. Grégori, D.E. Bergstrom, S. Fang, Y. Guan, K. Jennings, N. Gunaratna, Dyed microspheres for quantification of UV dose distributions: photochemical reactor characterization by Lagrangian actinometry, Journal of Environmental Engineering 132 (2006) 1390–1403.
[22] H. Funayama, T. Sugawara, Direct determination of absolute light intensity in UV-transmitting and UV-dispersive fluoro polymer tubes, Bulletin of the Chemical Society of Japan 60 (1987) 2245–2249.
[23] J.H. Lowry, J.S. Mendlowitz, N.S. Subramanian, Optical characteristics of the Teflon AF fluoro-plastic materials, Optical Surfaces Resistant to Severe Environments 1330 (1990) 142–151.
[24] J.A. Dever, C.A. McCracken, Effects of vacuum ultraviolet radiation of various wavelength ranges on Teflon FEP film, High Performance Polymers (2004) 289–301.
[25] A.A. Borovikov, G.N. Khlybov, M.I. Yakushin, Optical properties of Teflon at high temperatures, Journal of Applied Mechanics and Technical Physics 15 (1974) 516–520.
[26] G. Hougham, P.E. Cassidy, K. Johns, T. Davidson, Fluoropolymers 2: Properties, Plenum Press, New York, 1999.

[27] J.J. Ducoste, M.M. Clark, The influence of tank size and impeller geometry on turbulent flocculation: II Model, Environmental Engineering Science 15 (1998) 225–235.
[28] D.J. Greene, B. Farouk, C.N. Haas, CFD Design approach for chlorine disinfection processes, American Water Works Association 96 (2004) 138–150.
[29] M. Kamimura, S. Furukawa, J. Hirotsuji, Development of a simulation for ozone/UV reactor based on CFD analysis, Water Science and Technology 46 (2002) 13–19.
[30] S.M. Alpert, D. Knappe, J.J. Ducoste, Modeling the UV/hydrogen peroxide advanced oxidation process using computational fluid dynamics, Water Research (2009), doi:10.1016/j.watres.2009.12.003.
[31] R. Alexander-Katz, L. Ferry, G. Vigier, Interaction between UV radiation and filled polytetrafluoroethylene (PTFE). A multiple scattering analysis, Journal of Polymer Science: Part B: Polymer Physics 36 (1998) 2069–2083.
[32] G.R. Fowles, Introduction to Modern Optics, 2nd ed., Dover Publications Inc., New York, 1989, ISBN: 9780486659572, p. 336.
[33] R. Franke, W. Rodi, Calculation of vortex shedding past a square cylinder with various turbulence models, Turbulent Shear Flows 8 (1991).
[34] A. Sozzi, F. Taghipour, Computational and experimental study of annular photoreactor hydrodynamics, International Journal of heat and fluid flow 27 (2006) 1043–1053.
[35] W.P. Jones, B.E. Launder, The prediction of laminarization with a two-equation model of turbulence, International Journal of Heat Mass Transfer 15 (1972) 301–314.
[36] J. Boussinesq, Théorie de l'Ecoulement Tourbillant, Mem. Présentés par Divers Savants Acad. Sci. Inst. Fr. 23 (1877) 46–50.
[37] B.E. Launder, D.B. Spalding, The numerical computation of turbulent flows, Computer Methods in Applied Mechanics and Engineering 3 (1974) 269–289.
[38] J. Gregory, Particles in Water—Properties and Processes, IWA, 2005, p. 198, ISBN: 9781843391029.
[39] S. Chandrasekhar, Radiative Transfer, Dover Publications Inc., 1960, p. 393, ISBN: 0-486-60590-6.
[40] S.V. Patankar, Numerical Heat Transfer and Fluid Flow, Hemisphere Publishing Corporation, 1980, ISBN: 0891165223.
[41] EPA, Ultraviolet Disinfection Guidance Manual for the Final Long Term 2 Enhanced Surface Water Treatment Rule, U.S. Environmental Protection Agency, EPA 815-R-06-007, Cincinnati, OH, 2006.
[42] T.H. Cormen, C.E. Leiserson, R.L. Rivest, C. Stein, Introduction to Algorithms, 2nd ed., MIT Press and McGraw-Hill, 2001, ISBN 0-262-03293-7 Section 29.3: The simplex algorithm, pp. 790–804.
[43] ModeFrontier 3.0 User Manual, Esteco s.r.l., 2003.
[44] L.R. Koller, Ultraviolet Radiation, John Wiley & Sons Inc., New York, 1952, p. 270.
[45] H. Mamane-Gravetz, K.G. Linden, A. Cabaj, R. Sommer, Spectral sensitivity of Bacillus subtilis spores and MS2 coliphage for validation testing of ultraviolet reactors for water disinfection, Environmental Science and Technology 39 (2005) 7845–7852.
[46] A. Sozzi, F. Taghipour, UV reactor performance modeling by Eulerian and Lagrangian methods, Environmental Science and Technology 40 (2006) 1609–1615.